Applied Catalysis B: Environment and Energy 351 (2024) 124015

Contents lists available at ScienceDirect

Applied Catalysis B: Environment and Energy

journal homepage: www.elsevier.com/locate/apcatb

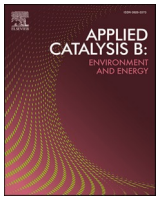

Biomineralization induced synthesis and self-assembly of photocatalyst-enzyme hybrid system for highly efficient environmental remediation

Yan-Zhai Wang [a], Syed Bilal Shah [a], Jun-Ying Liu [a], Hao Hu [d], Yang-Chun Yong [a,b,c,*]

[a] Biofuels Institute, Institute for Energy Research, School of Environment and Safety Engineering, Jiangsu University, 301 Xuefu Road, Zhenjiang 212013, China
[b] Jiangsu Collaborative Innovation Center of Technology and Material of Water Treatment, Suzhou University of Science and Technology, Suzhou 215009, China
[c] Nanchang Key Laboratory of Microbial Resources Exploitation & Utilization from Poyang Lake Wetland, College of Life Sciences, Jiangxi Normal University, Nanchang 330022, China
[d] School of Chemical and Pharmaceutical Engineering, Changzhou Vocational Institute of Engineering, 33 Gehu Middle Road, Changzhou 213164, China

ARTICLE INFO

Keywords:
Biomineralization
Photocatalyst-enzyme hybrid system
Organic dyes
Environmental remediation
Photocatalysis

ABSTRACT

The photocatalyst-enzyme hybrid systems (PEHSs) provided a promising method for environmental remediation by simultaneously harnessing the power of solar-energy conversion and biocatalysis. However, the use of PEHSs for environmental remediation was restricted by a complicated synthesis and assembly process. This work explored a simple one-pot biomineralization approach to fabricate PEHS. It was found that the cytochrome enzyme could be directly self-assembled onto the biosynthesized CdS during biomineralization by *Shewanella oneidensis* MR-1. More strikingly, those attached cytochrome enzymes could efficiently receive the photoelectrons from the CdS and serve as the photoreduction center which formed a typical PEHS. Impressively, this bio-CdS-cytochrome PEHS exhibited an extremely high photocatalytic decolorization rate of 69.4 mg/g/min, which was the highest record ever reported for procion red H-E3B. This work provided a simple and facile approach for PEHSs fabrication, which would be promising for practical application in environmental remediation.

1. Introduction

The photocatalyst-enzyme hybrid systems (PEHSs) that assembled by enzymes and photocatalysts, combined solar energy conversion capability, biocatalytic activity (high selectivity and activity) and thus was considered as one of the most promising systems to address energy and environmental issues [1–4]. In a typical PEHS, the photocatalyst generated photoinduced electrons under light irradiation, then these electrons were either converted into electron transport mediators or directly transferred to the enzymes for catalysis [3,5,6]. In direct contact mode, the photocatalysts bound to the enzymes, allowing the photoinduced electrons transferred directly to the catalytic site, which avoided the constraints of electron transport mediators [7]. By varying the types of enzymes, PEHSs could be applied for energy conversion [8,9], chemical synthesis [6,10], or environmental remediation [11,12].

According to the reaction characteristics, the basic units of PEHSs could be divided into enzyme and photocatalytic modules [1,3,13]. The vast majority of photocatalytic modules had been synthesized under complex and harsh conditions using chemical approaches [14-17]. Subsequently, photocatalytic modules were connected indirectly or directly to enzyme modules through mediators, physical adsorption, or chemical bonding [18-20]. Jiang et al. constructed a PEHS containing enzymes and CeO_2-$3TiO_2$ nanomaterials by fabricating CeO_2-$3TiO_2$ using a high-temperature/pressure and calcination method, and assembling the enzymes onto the CeO_2-$3TiO_2$ nanoparticles through physical adsorption [21]. Wilker et al. synthesized CdS nanorods in Ar atmosphere through multiple high-temperature reactions and complex ligand binding with purified hydrogenase [20]. During the chemical or physical assembly of enzymes with nanoparticles, the activity of enzymes might be irreversibly affected due to the poor biocompatibility of photocatalytic modules [3,5]. In addition, the traditional purification steps for enzymes were complex, expensive, and could potentially inhibit their catalytic activity [22,23]. Therefore, it was still desirable to develop a simple, biocompatible, and in-expensive fabrication method

* Corresponding author at: Biofuels Institute, Institute for Energy Research, School of Environment and Safety Engineering, Jiangsu University, 301 Xuefu Road, Zhenjiang 212013, China.
E-mail address: ycyong@ujs.edu.cn (Y.-C. Yong).

https://doi.org/10.1016/j.apcatb.2024.124015
Received 7 January 2024; Received in revised form 15 March 2024; Accepted 28 March 2024
Available online 29 March 2024

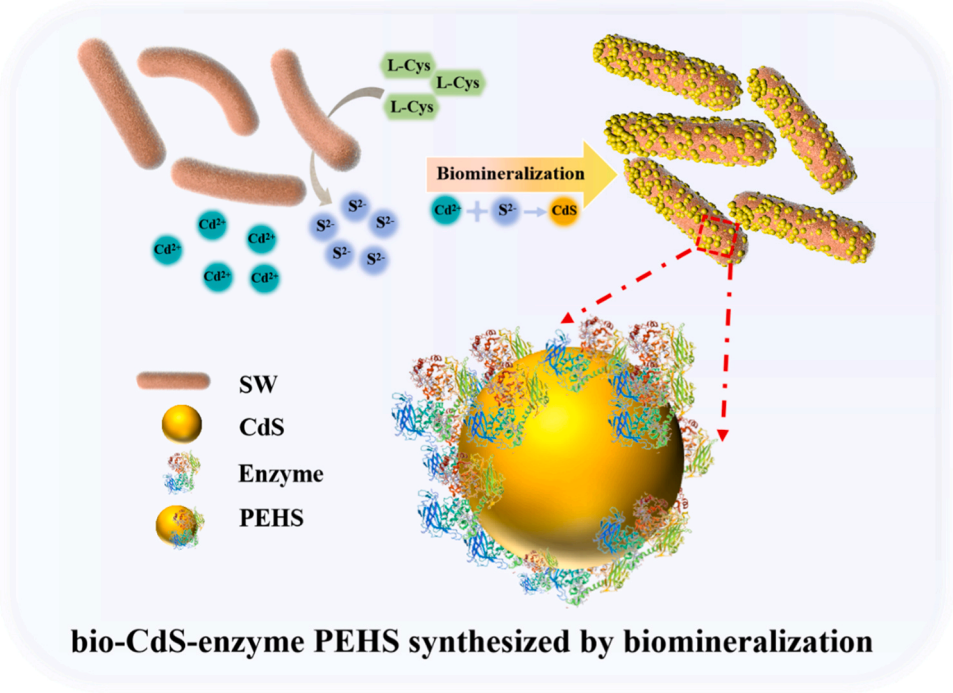

Fig. 1. Schematic illustration of PEHS synthesized by biomineralization.

for PEHSs.

Currently, many microorganisms [24,25], fungi [26,27], and plant extracts [28,29], were employed to synthesize biomaterials including monometallic/multicomponent composite metals [24,30], oxides [31], and sulfides [25]. Previous studies had showed that *E. coli* and *Shewanella* could synthesize photosensitive nanoparticles with excellent biocompatibility through biomineralization [25,32]. However, the reported studies focused on the photocatalytic characteristics of pure materials [25,27] or their interaction with whole-cell [32,33]. For whole-cell based hybrid systems (cells-photocatalysts), there was still a spatial obstacle for electron transportation between the photosensitive material and the biological enzyme, which would limit the photocatalytic activity of the hybrid systems. On the other hand, during the biomineralization process, microbial components including enzymes might be involved in the nucleation, orientation, and growth of inorganic minerals at the molecular level [34,35]. So, it was highly possible that enzymes were closely linked to nanomaterials during biomineralization. Thus, it was envisioned that the PEHSs might be fabricated using a biomineralization process to avoid the chemical synthesis of nanomaterials, eliminate the need for enzyme purification, and simplify the binding process for enzymes-nanomaterials.

Here, a new one-pot fabrication approach for PEHSs through biomineralization using the exoelectrogenic bacterium *S. oneidensis* MR-1 was reported (Fig. 1). The type of enzymes on the CdS surface was characterized and identified using cyclic voltammetry (CV), ultraviolet-visible full-wavelength scanning (UV–vis), Raman and Fourier infrared spectroscopy (FTIR). The cytochrome enzyme was identified as the active site of PEHS for photocatalytic decolorization. The application of PEHS in whole cells and the remediation of other environmental pollutants were presented. Finally, the electron transfer mechanism was investigated by adding related inhibitors, sacrificial agents, and biocatalysts. It was found that photoelectrons were produced by CdS, and thus were directly transported to the enzyme for efficient photocatalytic reactions. The discovery of this new method provided a reliable way for the synthesis of PEHS, and establishes a promising scheme for environmental remediation.

2. Materials and methods

2.1. Biosynthesis and self-assembly of bio-CdS-enzyme PEHS

Shewanella oneidensis MR-1 and cytochromes gene knockout strains (ΔMtrB and ΔMtrC/OmcA) [24] were aerobically inoculated in 10 mL LB medium under shaking (180 rpm) at 30°C for 12 h, 1 mL of the bacterial culture was transferred into 200 mL CdS synthesis medium (containing 8.5 g/L NaCl, 0.16 g/L $MgSO_4$, 0.56 g/L β-glycerophosphate·2Na, 0.4 g/L NH_4Cl, 0.25 g/L KCl, 0.05 g/L $CaCl_2$, 10 g/L 3-(N-Morpholino) propanesulfonic acid (MOPS), 0.3 mM $CdCl_2$, 1 mM L-cysteine, 0.2 g/L peptone, 0.1 g/L yeast extract, and 10 mM sodium lactate, pH = 7.2) [25]. The bacteria were then grown aerobically for the production of CdS under 180 rpm shaking at 30 °C. After 12 h, the yellow pellets were collected by centrifugation at 3000 rpm for 5 min and used for the isolation of bio-CdS-enzyme PEHS.

2.2. Isolation of bio-CdS-enzyme PEHS and chemical synthesis of CdS nanoparticles

The collected yellow pellets in Section 2.1. were ultrasonicated for 1 h to disrupt the cells. Centrifugation (10,000 rpm, 10 min) was then applied to remove cell debris as the precipitates. The supernatant was further centrifuged at 17,000 rpm for 30 min to obtain a yellow bio-CdS-enzyme precipitation. After three rounds of washing with pure water, the bio-CdS-enzyme PEHS was obtained. For the validation of enzyme activity or the preparation of enzyme-free bio-CdS, the bio-CdS-enzyme PEHS was treated with 100 mg/L protease K (37°C, 12 h) and 10% sodium dodecyl sulfate (SDS) to remove enzymes that were attached to the surface of CdS. Then, the solution was centrifuged at 17,000 rpm for 30 min to obtain a yellow CdS precipitation. It was washed three times with pure water and designated as treated bio-CdS. The collected bio-CdS-enzyme PEHS or treated bio-CdS was freeze-dried and stored in the dark at room temperature.

Chemical synthesis of CdS nanoparticles was prepared by mixing 16.2 mM $Cd(NO_3)_2{\bullet}4H_2O$ with 48.6 mM thiourea in 40 mL ethylenediamine, then heating in a hydrothermal synthesis reactor at 160°C

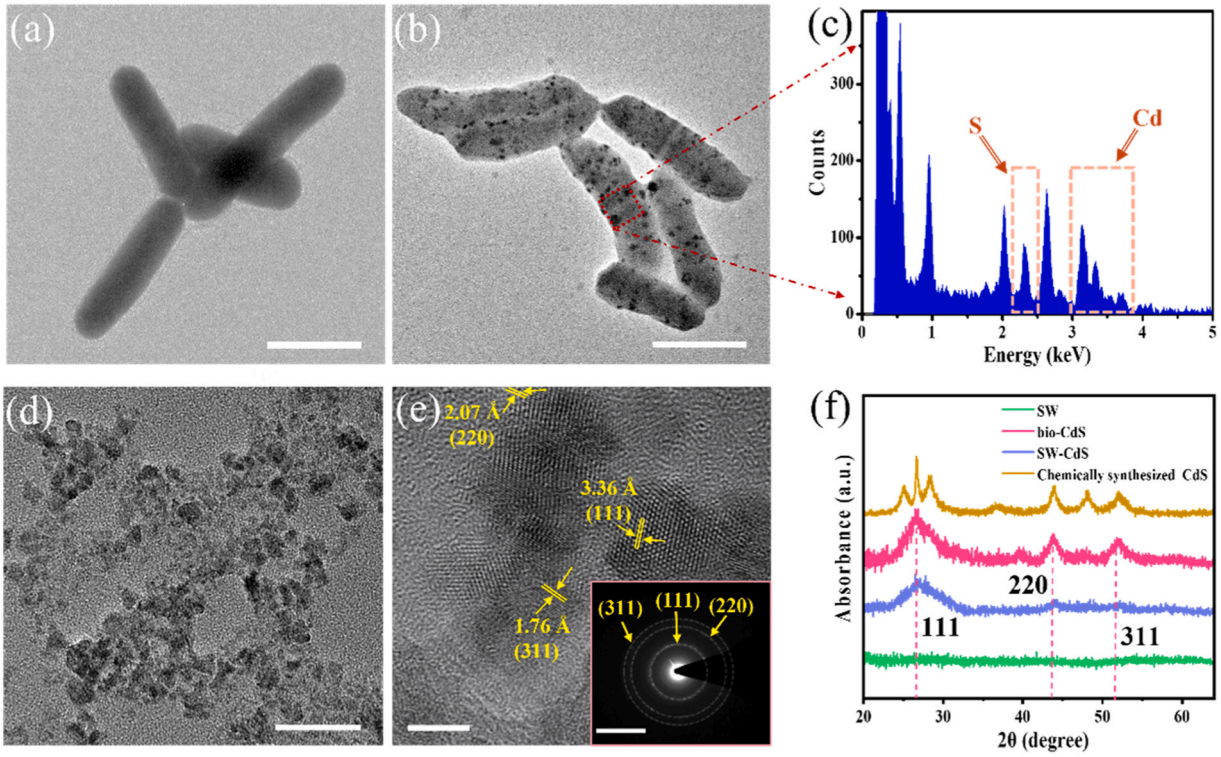

Fig. 2. TEM images of (a) SW cell, (b) bio-CdS synthesized by SW. (c) EDS spectrum of select area in (b). (d) HRTEM image of isolated bio-CdS nanoparticles. (e) HRTEM image and selective area electron diffraction (SAED) analysis of isolated bio-CdS nanoparticles. (f) XRD of SW cell, SW-CdS (without isolation), isolated bio-CdS, and chemically synthesized CdS. Scale bars: (a), (b) 1 μm; (d) 50 nm; (e) 5 nm; inset of (e) 5 1/nm. The inset of (e) shows an SAED analysis of nanoparticles.

for 12 h. After the hydrothermal reaction, the products were cleaned with pure water and ethanol. Subsequently, the samples were freeze-dried and stored in the dark at room temperature [32].

2.3. Characterization of bio-CdS-enzyme PEHS

For the microscopic morphology and element analysis of the whole-cell PEHS, the hybrid system was processed with the following sequence: resuspended in 0.1 M phosphate-buffered saline solution (PBS) and then fixed with 2.5% glutaraldehyde at room temperature for fixation (4 h), washed twice with 0.1 M PBS, dehydrated successively in 50%, 70%, 80%, 90%, 95%, and 100% (3 times) ethanol for 15 min each time [24]. For scanning electron microscopy (SEM) observation and energy-dispersive X-ray spectroscopy (EDS) analysis, the dehydrated samples were dripped onto the silicon wafer, after air-dried, sputtered by gold, and then observed using a field emission scanning electron microscope (JSM-7800 F, JEOL, Japan). For high-resolution transmission electron microscopy (HRTEM) observation and EDS analysis, the samples of the dehydrated whole cells and the bio-CdS-enzyme PEHS were dripped onto the copper grid. After air-drying, the samples were observed using high-resolution transmission electron microscopy (TF-G20, Thermo Scientific, USA). The bacteria, bio-CdS-enzyme PEHS, chemically synthesized CdS, and treated bio-CdS were characterized using various analytical techniques: X-ray photoelectron spectroscopy (Escalab 250Xi XPS, Thermo Scientific, USA), X-ray diffractometer (D8 Advance, Bruker, Germany), Raman spectrometer (DXR Microscope, Thermo Scientific, USA), UV–vis diffuse reflectance spectrometer (UV-3600 spectrometer, Shimadzu, Japan), and FTIR spectrometer (ALPHA II, Bruker, Germany).

2.4. Photocatalytic activity determination

The final concentration of 100 mg/L procion red H-E3B (PR H-E3B) or other pollutants was added to the photocatalytic system (12 mg/L catalyst/OD_{600}=0.2 SW-CdS, 10 mL of 0.1 M PBS containing 10 mM Na_2SO_3) under various reaction conditions using simulated sunlight (50 W LED light source). At regular intervals, 1 mL of the reaction samples was collected into centrifuge tubes using syringes. The volume ratio of 1:1 hydrochloric acid was added for the termination reaction, and liquid samples containing pollutants were obtained after centrifugation (5000 rpm, 10 min) for quantitative analysis.

The photodegradation mechanism of PEHS was clarified by adding 0.01/0.05/0.1 mM riboflavin/methyl viologen as electron transport mediators [36], 20 mM Na_2SO_3 as photogenerated hole scavengers, 20 mM methanol (MET) and isopropanol (IPA) as photogenerated ·OH scavengers, and 20 mM ammonium oxalate (AO) as photogenerated h^+ scavengers [37]. Additionally, 0.5 mM hexavalent chromium (Cr^{6+}) was added as an electrons capturer [32].

2.5. Analytical method

The concentrations of PR H-E3B and methyl orange (MO) were determined at 540 nm and 480 nm, respectively, using a UV–vis spectrophotometer (WPA Biowave II, Biochrom, UK) [38,39]. The concentration of $K_2Cr_2O_7$ (Cr^{6+}) was determined using the carbohydrazide spectrophotometric method [40]. CV analyses were conducted by using a CHI660E electrochemical workstation (CHI, Shanghai, China) with a glassy carbon electrode as the working electrode, a platinum wire as the counter electrode, and a saturated calomel electrode as the reference electrode.

2.6. Computation methods of DFT calculations

Spin-unrestricted calculations were performed using $DMol^3$ code within density function theory (DFT). The Perdew-Burke-Ernzerhof (PBE) functional was adopted to describe the exchange and correlation potential. Effective core potentials treated core electrons, and a double numerical plus polarization (DNP) basis set described atomic

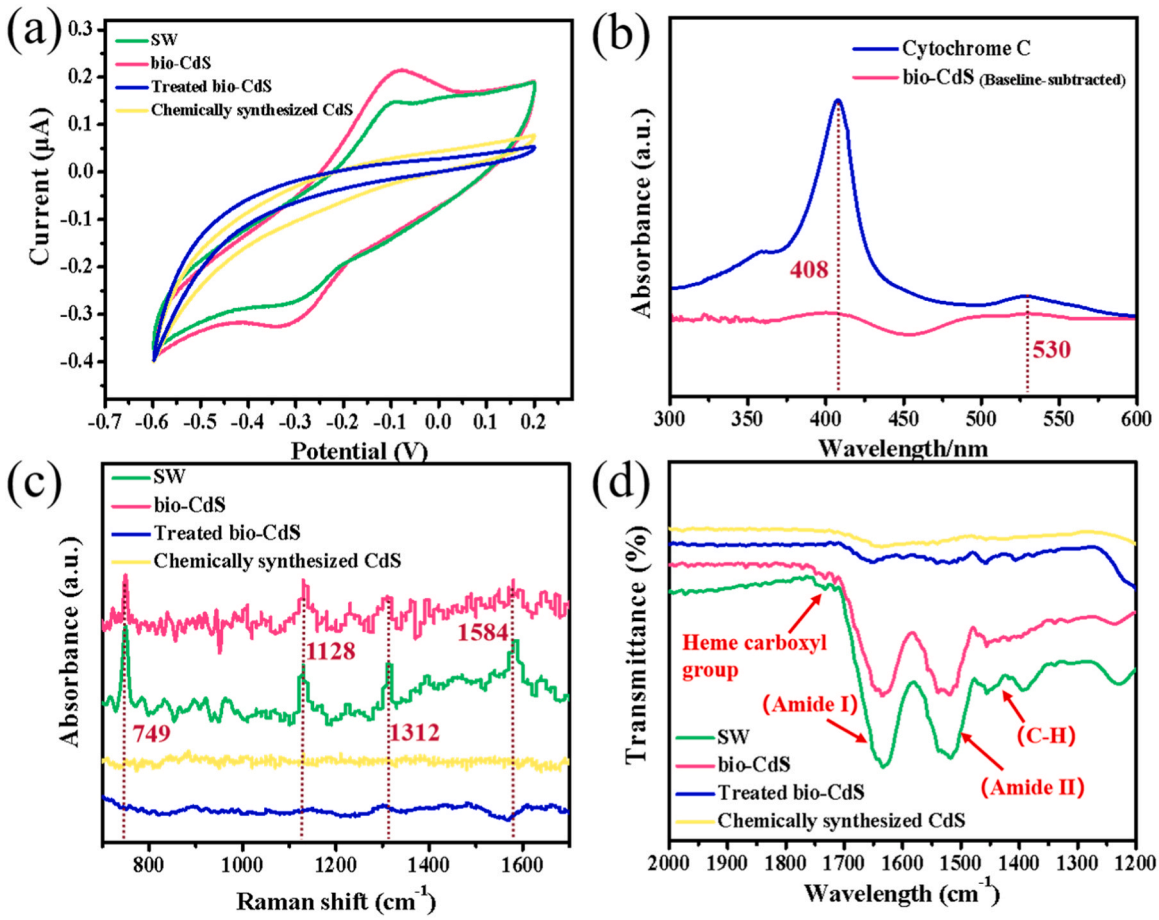

Fig. 3. (a) Cyclic voltammetry scanning of SW cell, isolated bio-CdS, treated bio-CdS, and chemically synthesized CdS. (b) The baseline-subtracted UV–vis spectra of pure cytochrome C and isolated bio-CdS (The original spectra were shown in Fig. S5). (c) Raman and (d) FTIR spectra of SW cell, isolated bio-CdS, treated bio-CdS, and chemically synthesized CdS.

orbitals. A global orbital cut-off radius of 5.2 Å ensured high precision. Van der Waals interactions were described by DFT + D2 method. The smearing value was set at 0.001 Ha. Convergence tolerances of energy, maximum displacement and maximum force were 1.0×10^{-5} Ha, 0.005 Å and 0.002 Ha/Å, respectively.

In this work, atomic-scale simulation was conducted on a three-layer 3 × 4 CdS slab with the bottom two layers fixed in bulk positions (24.74 × 23.33 ×6.24 $Å^3$). A 25 Å vacuum layer was added to avoid the periodic interaction. The Heme 10−CdS interface was modeled by adding Heme 10 above the slab. This model contains 221 atoms and the *k*-space was sampled by the Gamma point. Furthermore, the HSE06 hybrid functional in the CASTEP module was utilized for a rational calculation of the bulk CdS band structure with a 4 × 4 × 4 *k*-mesh.

3. Results and discussion

3.1. One-pot biosynthesis and self-assembly of bio-CdS-enzyme

To fabricate an efficient photocatalyst-enzyme hybrid system (PEHS), cadmium sulfide (CdS) was chosen as the photosensitizer in the PEHS due to its high visible light photocatalytic activity and suitable energy band location for photocatalytic environmental remediation and energy production [41,42]. *S. oneidensis* MR-1 (SW) was one of the model strains for environmental remediation, it was rich in various cytochrome enzyme and other enzymes for degrading or reducing pollutants [43]. Furthermore, SW was also a model metal-reducing bacterium with efficient biomineralization capability for the biosynthesis of various nanoparticles [24,25]. Thus, a biosynthesis approach for CdS nanoparticle fabrication with SW was designed using cadmium ($CdCl_2$) and sulfur (L-cysteine) as the precursors (Fig. 1). Upon the mixing of SW with these precursors, the mixture gradually turned to a bright yellow color (Fig. S1a), and SW showed high cell viability in the mixture (Fig. S1e). On the other hand, the bacterial culture without these precursors didn't exhibit such a color change. This result suggested that SW might produce CdS that featured as yellow color. Thus, the bacterial cells after incubation with those precursors were characterized with scanning electron microscopy (SEM), high-resolution transmission electron microscopy (HRTEM), and energy-dispersive X-ray spectroscopy (EDS) analysis. According to the SEM and HRTEM observation, the surface of bacterial cells without precursors was smooth and devoid of any particles (Figs. 2a and S1b), whereas the surface of bacterial cells incubated with those precursors was evenly distributed with nanoparticles (Figs. 2b and S1c). Further, the presence of Cd and S elements was identified in these nanoparticles attached to the surface of the bacterial cells (Figs. 2c and S1d), indicating that these nanoparticles might be CdS synthesized by SW.

The crystallographic structure of the biosynthesized CdS (bio-CdS) was determined by X-ray diffraction (XRD) (Fig. 2f). The XRD results revealed a typical pattern identical to pure CdS (JCPDS#10–0454), consisting of two sharp peaks at 2θ = 43.9° (220) and 52.1° (311), along with a broad peak at 2θ = 26.5° (111). It was further confirmed by HRTEM image and its selective area electron diffraction (SAED) analysis (Fig. 2d and e). Moreover, the nanoparticles were characterized as CdS by XPS (Fig. S2) and Raman spectroscopy (Fig. S3c) analyses. According to the UV–vis diffuse reflectance spectrum (DRS) and absorption spectra of bio-CdS (Fig. S3a and b), the valence electron energy transition of bio-

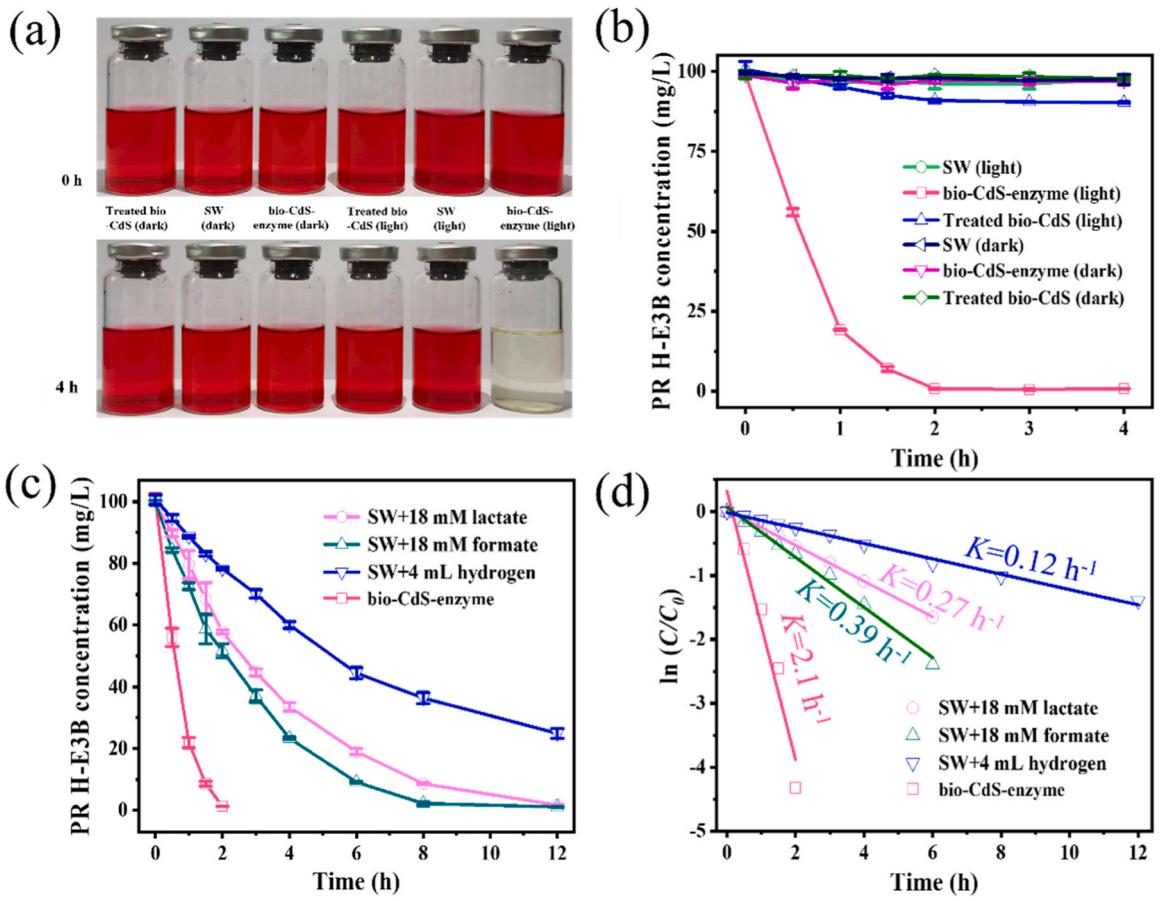

Fig. 4. (a) Photograph of photocatalytic decolorization of procion red H-E3B (PR H-E3B) by different catalysts. (b) Photocatalytic decolorization of PR H-E3B under different conditions. Na_2SO_3 (10 mM) was used as the hole sacrificial agent. (c) Comparison of photo-decolorization of PR H-E3B by isolated bio-CdS and metabolic decolorization by SW cell (OD_{600}=0.2) with different electron donors. (d) The pseudo-first order kinetic fitting of (c).

CdS nanoparticles was detected in the visible region of the solar spectrum (Eg=2.38 eV, $\lambda_{absorption}$=410 nm) (Fig. S3d) [44–46], confirming the visible-light photocatalytic ability of bio-CdS synthesized by SW. Furthermore, bio-CdS was verified as a direct semiconductor using DFT calculations (Fig. S4), well aligned with our experimental results previous study [47].

Moreover, the bio-CdS was characterized by cyclic voltammetry (CV), ultraviolet-visible full-wavelength scanning (UV–vis), Raman and Fourier transform infrared spectroscopy (FTIR) (Fig. 3). For bio-CdS, the CV results showed a peak pair representing the cytochrome enzyme around −0.219 V, which was similar to that from SW (Fig. 3a) [24]. UV–vis absorption spectra of bio-CdS and cytochrome C exhibited similar characteristic peaks at 408 nm and 530 nm (Fig. 3b). But the chemically synthesized CdS and treated bio-CdS (treated with protease K and sodium dodecyl sulfate (SDS) to remove enzymes) did not exhibit the similar characteristic peaks representing cytochrome enzymes in CV and UV–vis. The C-type cytochrome signature bands at 749 cm^{-1} (pyrrole breathing mode), 1128 cm^{-1} (ν(CN) tensile vibration), 1312 cm^{-1} (δ(CH) deformation), and 1584 cm^{-1} (ν(CC) skeletal stretches) were also observed in the Raman spectra of SW and bio-CdS (Fig. 3c). According to previous reports, the four Raman bands at 749, 1128, 1312, and 1584 cm^{-1} were the typical spectra of C-type cytochrome enzyme found in *Geobacter* [48,49] and SW [50]. Furthermore, the chemically synthesized CdS and treated bio-CdS did not exhibit these distinctive peaks. In addition, the bio-CdS and SW showed prominent FTIR band at ~1741 cm^{-1} attributed to the stretching vibration of carboxyl groups from heme, the band at ~1640 cm^{-1} attributed to the amide I stretching vibration of carbonyl groups from peptide bonds, the band at ~1540 cm^{-1} attributed to the protein amide N−H bonds, and the region from ~1450 cm^{-1} representing C−H bending vibrations of amino acid side chains (Fig. 3d) [48]. These results indicated the coexistence of cytochrome enzymes with the bio-CdS, confirming a bio-CdS-enzyme system was successfully synthesized and self-assembled by SW, which would potentially serve as a new biosynthesized PEHS.

3.2. Photocatalytic activity of bio-CdS-enzyme PEHS

To further verify the feasibility of utilizing the biosynthesized bio-CdS-enzyme as PHES, the photocatalytic activity of bio-CdS-enzyme was assessed in a photocatalytic decolorization system. Firstly, the pH and sacrificial agent for the photocatalytic decolorization were optimized (Figs. S6 and S7). Under visible light irradiation, bio-CdS-enzyme exhibited a good dye decolorization capacity (Fig. 4a), as evidenced by the characteristic peaks of dyes (510 nm and 540 nm) decreasing with time and eventually disappearing after 2 h (Fig. S8a). In detail, the azo dye (100 mg/L) was decolorized by approximately 81% after 1 h and completely decolorized within 2 h by bio-CdS-enzyme, while no decolorization of the azo dye occurred under dark conditions (Fig. 4b). On the contrary, the treated bio-CdS (enzymes removed) only showed ~10% removal within 2 h. Next, the kinetics of dye decolorization were analyzed using a pseudo-first order kinetic model (Fig. S9). The fitted rate constant (k) was 2.23 h^{-1} and 0.07 h^{-1} for bio-CdS-enzyme, respectively. The bio-CdS-enzyme exhibited a photocatalytic decolorization efficiency (k) at least 31.8 times higher than treated bio-CdS (enzymes removed). After photocatalytic decolorization, the structural of bio-CdS-enzyme PEHS was analyzed using Raman and FTIR spectroscopy. The characteristic peaks representing the cytochrome enzymes were essentially unchanged (Fig. S10), so the structure of the enzymes in

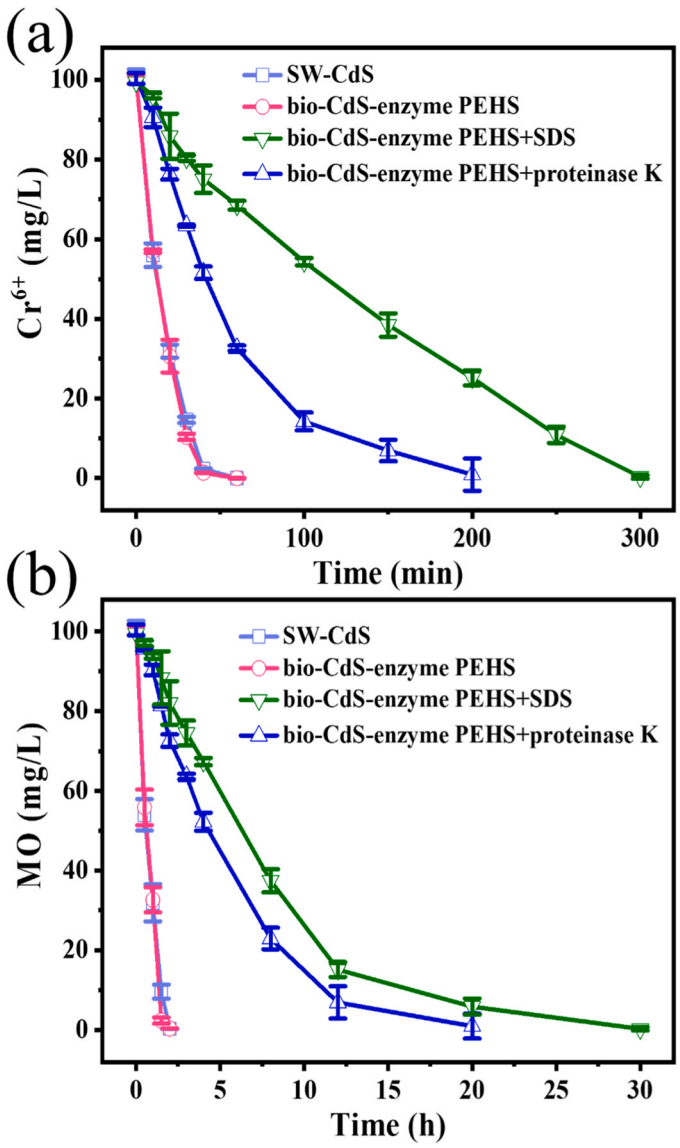

Fig. 5. (a) Photocatalytic reduction of Cr^{6+} under different conditions. (b) Photocatalytic decolorization of methyl orange (MO) under different conditions.

PEHS was stable during photocatalytic decolorization. The catalytic stability of bio-CdS-enzyme was also demonstrated in terms of photocatalytic decolorization using the four repeated experiments employing the recycled bio-CdS-enzyme photocatalyst (Fig. S8b). The results indicated that bio-CdS-enzyme exhibited excellent photocatalytic activity, and the enzymes attached to bio-CdS played an important role in the photocatalysis of bio-CdS-enzyme, confirming that bio-CdS-enzyme was a typical PHES.

The photocatalytic decolorization activity of the biosynthesized bio-CdS-enzyme PEHS was compared with SW metabolic decolorization and other nanomaterials' photocatalytic decolorization. As shown in Fig. 4c, SW exhibited the highest metabolic decolorization efficiency when sodium formate was used as the electron donor, resulting in complete decolorization of azo dyes within 8 h. However, the fitted rate constants (k) were 2.1 h^{-1} and 0.39 h^{-1} for bio-CdS-enzyme PEHS and SW metabolic decolorization, respectively. In Fig. 4d, bio-CdS-enzyme PEHS (photocatalysis) demonstrated a decolorization efficiency (k) at least 5.4 times higher than SW (metabolism). More impressively, compared with other nanomaterials, the bio-CdS-enzyme PEHS exhibited the highest photocatalytic decolorization rate towards the model organic dye of procion red H-E3B (PR H-E3B) (Table S1). The application of bio-CdS-enzyme PEHS in the remediation of other environmental pollutants was also evaluated. For the photocatalytic reduction of Cr^{6+} (Fig. 5a), bio-CdS-enzyme PEHS could completely reduce 100 mg/L of Cr^{6+} in 60 min. In comparison, treated CdS (enzymes removed) took 200 and 300 min to completely Cr^{6+}reduction, respectively. For other photocatalytic decolorization (Fig. 5b), bio-CdS-enzyme PEHS could completely decolorize methyl orange (MO) within 2 h, while the complete decolorization times of treated bio-CdS (enzymes removed) were delayed to 20 and 30 h, respectively. These findings further supported the important role of the cytochrome enzymes in PEHS.

To explore the photocatalytic activity of the whole-cell containing bio-CdS-enzyme PEHS without isolation (SW-CdS), various physicochemical methods were employed in SW-CdS for photocatalytic decolorization (Fig. S11). Compared to the catalytic activity of the whole-cell SW-CdS, the photocatalytic decolorization activity did not decrease when the bacteria were disrupted using ultrasound and lysozyme. This result demonstrated that the high photocatalytic activity of bio-CdS-enzyme PEHS was not caused by the integrality or activity of the bacteria. Conversely, the addition of enzyme inhibitors (protease K and SDS) greatly reduced the photocatalytic activity of whole-cell SW-CdS. Conversely, SDS [51,52] had the most significant inhibitory effect on the efficiency of photocatalytic decolorization, only ~25% of the dye was decolorized in 2 h. On the other hand, the remediation efficiency of other environmental pollutants (Cr^{6+} and MO) by whole-cell SW-CdS was nearly identical to that of the isolated bio-CdS-enzyme PEHS (Fig. 5). In particular, the PEHS retained almost all of its catalytic activity in the whole cells (SW-CdS) compared to that of the isolated hybrid system (bio-CdS-enzyme PEHS). This result showed that whole-cell PEHS was simpler and more energy saving because the PEHS in the whole cell could further simplify the production steps of the PEHS. In addition, when various electron donors were added to SW-CdS (Fig. S12), the catalytic efficiency did not change significantly, so the electrons required for enzymes catalysis were all from the photogenerated electrons by photocatalysis. These results indicated that the bio-CdS-enzyme PEHS synthesized without isolation also showed similar photocatalytic activity to the isolated system, suggesting that it could be further used as an isolation-free system for practical applications.

3.3. *Mechanism of photocatalytic decolorization by bio-CdS-enzyme PEHS*

The cytochrome enzymes of SW was one of the main catalysts for bioremediation [43], the knockout of the cytochrome enzymes' genes could affect the expression of cytochrome enzymes and thus affect the catalytic efficiency [24,53]. In this study, the metabolic decolorization efficiency of SW was significantly reduced, only less than 20% decolorization was achieved by cytochrome gene engineered knockout strains (membrane cytochrome enzymes MtrBC/OmcA) within 48 h (Fig. S13a). The results suggested that the cytochrome enzymes of MtrBC/OmcA were responsible for dye decolorization [53], implying that these enzymes might be the cytochromes attached to bio-CdS-enzyme PEHS. Thus, the photocatalytic activity of the bio-CdS-enzyme PEHSs synthesized by cytochrome enzyme mutant strains was evaluated and compared. For the mutant of ΔMtrC/OmcA strain, the synthesized bio-CdS-enzyme PEHSs should be free of cytochrome of MtrC/OmcA [24]. Interestingly, it was found that the ΔMtrC/OmcA-bio-CdS-enzyme PEHS (synthesized by the mutant of ΔMtrC/OmcA strain) showed a decreased decolorization rate (~17%), and the ΔMtrB-bio-CdS-enzyme PEHS (synthesized by the mutant of ΔMtrB strain) showed a decreased decolorization rate (~24%) (Fig. S13b), suggesting that these enzymes were important for bio-CdS-enzyme PEHSs. Therefore, these results substantiated that different cytochrome enzymes such as MtrB, MtrC, and OmcA, served as the functional components of this biosynthesized bio-CdS-enzyme PEHSs.

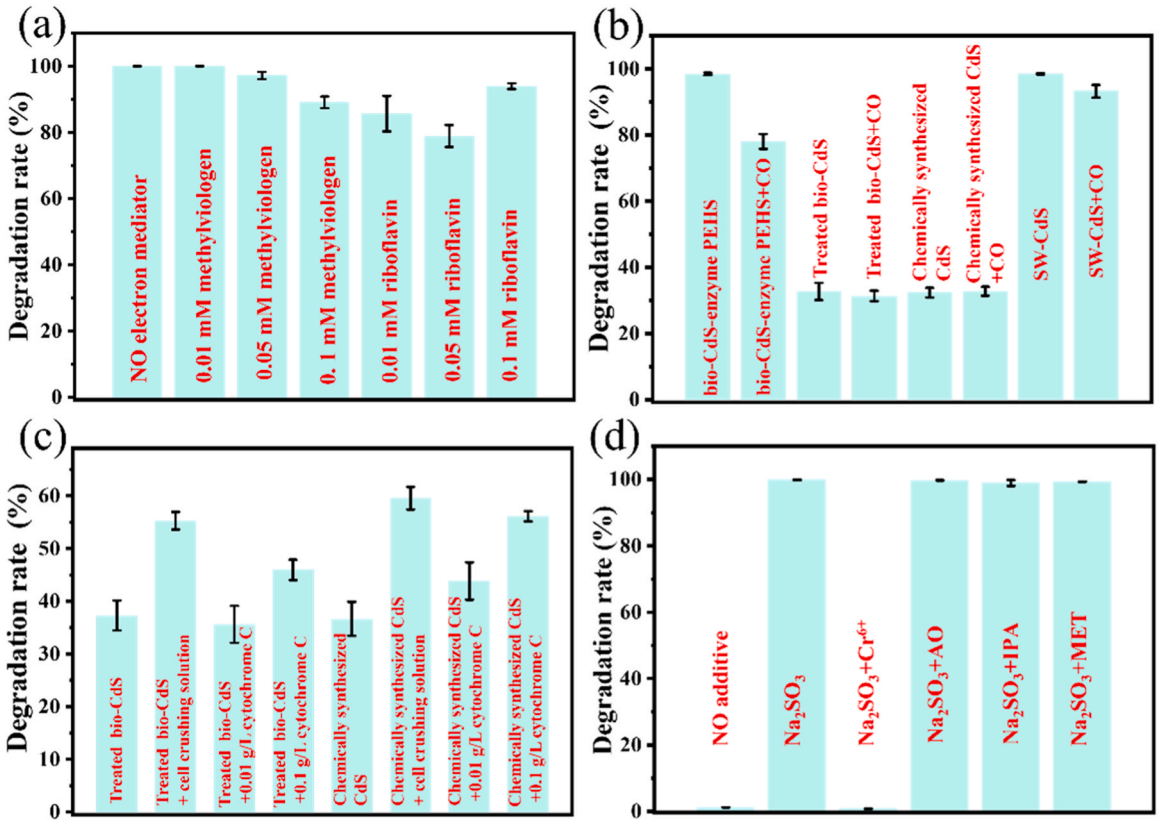

Fig. 6. Photocatalytic decolorization of PR H-E3B by bio-CdS-enzyme PEHS with (a) different kinds of electron transport mediators, (b) cytochrome enzyme inhibitor (10% CO). Effect of (c) cell crushing solution (produced by 1 mL SW cell (OD_{600}=2.0) under ultrasonic crushing) or pure cytochrome C, (d) photogenic electron inhibitors and different sacrificial agents on photocatalytic decolorization of PR H-E3B by bio-CdS-enzyme PEHS.

According to previous reports, the addition of organic electron transport mediators such as methylviologen (MV^{2+}) and riboflavin (VB_2) could significantly enhance the photocatalytic activity of the whole cell hybrid systems [36,54]. However, it was interesting that the addition of electron transport mediators did not improve the catalytic efficiency of PEHS, but decreased the photocatalytic efficiency when different concentrations of electron transport mediators were added (Fig. 6a). It was speculated that due to the direct contact between the photosensitive nanoparticles and the enzyme, the photogenerated electrons could be transferred directly to the enzyme without the need for electron transfer mediators. The addition of electron transfer mediators may competitively capture the photogenerated electrons from the photosensitive nanoparticles and hinder the normal process of electron transfer. Thus, the photocatalytic activity was affected by the addition of

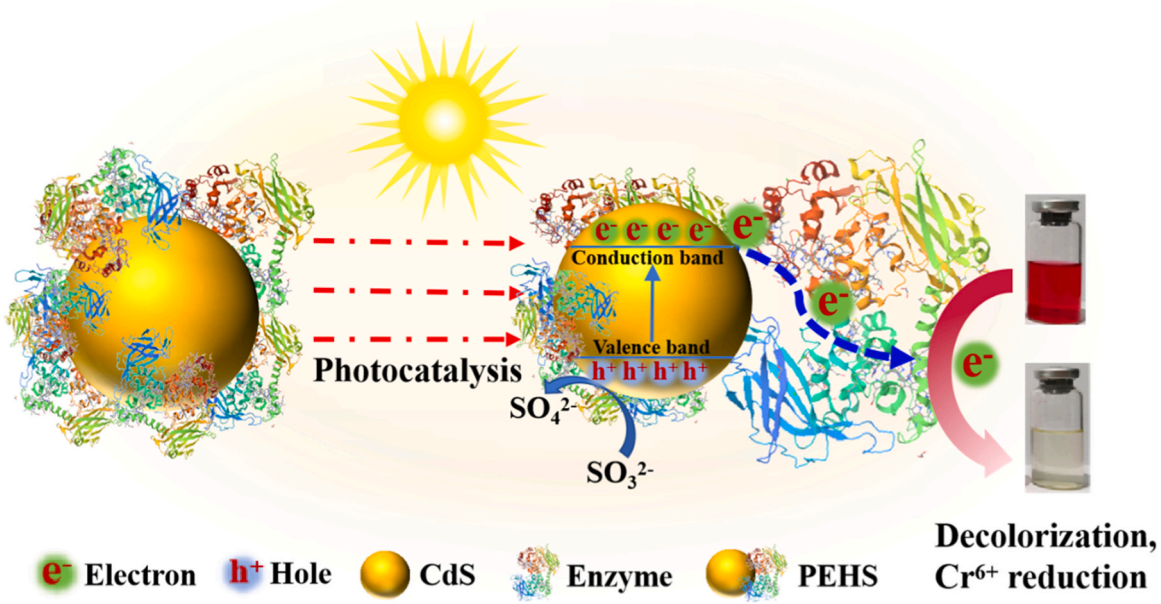

Fig. 7. Proposed mechanism of photo-catalytic decolorization by bio-CdS-enzyme PEHS.

electron transport mediators. In addition, to further analyze the surface enzyme of CdS, carbon monoxide (CO), as a particular cytochrome enzyme inhibitor [55,56], was added to bio-CdS-enzyme PEHS. As shown in Fig. 6b, the decolorization rates of bio-CdS-enzyme PEHS and SW-CdS were significantly inhibited by ~20% and ~5%, respectively. By adding cytochrome enzymes from cell crushing solution and 0.1 g/L cytochrome C into the photocatalytic decolorization system (Fig. 6c), the rates of photocatalytic decolorization of treated bio-CdS were increased by ~18% and ~8%, respectively. And the rates of photocatalytic decolorization of chemically synthesized CdS were increased by ~23% and ~19%, respectively. These results indicated that cytochrome enzymes play a major catalytic function on the bio-CdS surface during the photocatalytic decolorization.

In addition, the photocatalytic mechanism was further explored (Fig. 6d). Through the radical capture experiment, it was found that the bio-CdS-enzyme PEHS with hole sacrificial agent (Na_2SO_3) significantly improved the photocatalytic efficiency compared to that without sacrificial agent (Na_2SO_3). However, the addition of ammonium oxalate/isopropanol/methanol (AO/IPA/MET) as standard free radical scavengers did not affect decolorization efficiency, indicating that photogenerated species were not the cause of photocatalytic decolorization. The addition of Cr^{6+} (electrons capturer) severely inhibited the photocatalytic activity, indicating that the photogenerated electrons played a significant role in the decolorization process. These results indicated that the tight contact between CdS and enzymes enhanced the separation of electrons and holes pairs, and the suppression of holes with the use of the hole sacrificial agent (such as Na_2SO_3), which was beneficial for the photocatalytic reaction of bio-CdS-enzyme PEHS. At the same time, it also revealed the electron transport pathway of bio-CdS-enzyme PEHS that the electrons generated by bio-CdS transferred to enzymes for photocatalysis (Fig. 7).

To investigate the separation and transfer of photogenerated charge carriers in the bio-CdS-enzyme PEHS, the steady-state photoluminescence (PL) spectra of bio-CdS-enzyme PEHS and treated CdS were measured and analyzed. The steady-state PL intensity of bio-CdS-enzyme decreased in comparison with that of treated CdS (Fig. S14a), suggesting that the separation of the photoinduced electron−hole pairs in bio-CdS was greatly enhanced owing to the introduction of enzymes. That was further confirmed by electrochemical impedance spectroscopy and transient photocurrent response (Fig. S14b-c).

Density Functional Theory (DFT) calculations were employed to further elucidate the mechanisms of charge transfer between bio-CdS and the cytochrome enzymes. It is well-known that Heme 10 on the surface of cytochrome enzymes of *Shewanella oneidensis* MR-1 utilizes its Fe atom to accept photoinduced electrons, acting as a biocatalytic active site [36]. As depicted in Fig. S15, the distance between the Fe atom in Heme 10 and CdS was found to be as short as 3.45 Å. This distance was not only sufficient for direct electron transfer (<14 Å) but also suggested direct contact between CdS and the cytochrome enzymes. Additionally, Hirshfeld charge population analysis revealed efficient electron transfer (0.30 e) from CdS to Heme 10, with some accumulating on the Fe atom, as evidenced by the charge density difference (Fig. S15). These findings suggested that the attached cytochrome enzymes can effectively receive photoelectrons from CdS, serving as the photoreduction center in the formation of a typical PEHS.

4. Conclusions

In summary, a novel one-pot biosynthesis and self-assembly method for PEHS fabrication was developed. The bio-CdS was synthesized through biomineralization by *S. oneidensis* MR-1 using $CdCl_2$ and L-cysteine as the precursors under aerobic condition. During this biomineralization process, the enzyme was attached to the surface of bio-CdS nanoparticles, while the enzymes was identified as the cytochrome protein. Further analysis indicated that the bio-CdS and surface-attached enzymes formed an active PEHS with excellent electron transfer between CdS and the enzymes. Impressively, the cytochrome enzyme served as the reduction center by up-taking the photoelectrons from CdS, which dramatically promoted the photocatalytic decolorization of organic dyes by bio-CdS. In addition, this bio-CdS-cytochrome PEHS exhibited excellent catalytic activity in whole-cell which further exempted the time-consuming isolation process for PEHS fabrication. This work demonstrated the potential of bio-fabrication for PEHSs, which was expected to inspire new ideas and new applications for solar energy conversion or environmental remediation by PEHSs.

CRediT authorship contribution statement

Hao Hu: Data curation, Formal analysis. **Jun-Ying Liu:** Writing – review & editing, Methodology, Formal analysis. **Yang-Chun Yong:** Writing – review & editing, Visualization, Supervision, Resources, Project administration, Funding acquisition. **Yan-Zhai Wang:** Writing – original draft, Investigation, Formal analysis, Data curation, Conceptualization. **Syed Bilal Shah:** Investigation, Formal analysis.

Declaration of Competing Interest

The authors declare that they have no known competing financial interests or personal relationships that could have appeared to influence the work reported in this paper.

Data availability

Data will be made available on request.

Acknowledgments

This work was supported by National Natural Science Foundation of China (52170081), Natural Science Foundation of Jiangsu Province (Carbon Neutralization, BK20220003).

Appendix A. Supporting information

Supplementary data associated with this article can be found in the online version at doi:10.1016/j.apcatb.2024.124015.

References

[1] S. Zhang, S. Liu, Y. Sun, S. Li, J. Shi, Z. Jiang, Enzyme-photo-coupled catalytic systems, Chem. Soc. Rev. 50 (2021) 13449–13466.
[2] P.T. Fard, S.K. Albert, J. Ko, S. Lee, S.-J. Park, J. Kim, Spatial organization of photocatalysts and enzymes on Janus-type DNA nanosheets for efficient CO_2 conversion, ACS Catal. 12 (2022) 9698–9705.
[3] N. Yang, Y. Tian, M. Zhang, X. Peng, F. Li, J. Li, Y. Li, B. Fan, F. Wang, H. Song, Photocatalyst-enzyme hybrid systems for light-driven biotransformation, Biotechnol. Adv. 54 (2022) 107808.
[4] H. He, X. Gao, K. Xu, H. Li, Y. Hu, C. Yang, F. Fu, 1D/0D Z-scheme heterostructure of $Bi_2S_3/Cd_XZn_{1-X}S$ with strong interfacial electric field coupling enhanced mass transfer based on gas-liquid-solid micro interface contact for efficient photothermal synergistic catalytic CO_2 reduction to syngas, Chem. Eng. J. 450 (2022) 138266.
[5] S.H. Lee, D.S. Choi, S.K. Kuk, C.B. Park, Photobiocatalysis: activating redox enzymes by direct or indirect transfer of photoinduced electrons, Angew. Chem. Int. Ed. 57 (2018) 7958–7985.
[6] L. Schmermund, V. Jurkaš, F.F. Özgen, G.D. Barone, H.C. Büchsenschütz, C. K. Winkler, S. Schmidt, R. Kourist, W. Kroutil, Photo-biocatalysis: biotransformations in the presence of light, ACS Catal. 9 (2019) 4115–4144.
[7] S.H. Lee, D.S. Choi, M. Pesic, Y.W. Lee, C.E. Paul, F. Hollmann, C.B. Park, Cofactor-free, direct photoactivation of enoate reductases for the asymmetric reduction of C═C bonds, Angew. Chem. Int. Ed. 129 (2017) 8807–8811.
[8] B. Chica, C.-H. Wu, Y. Liu, M.W. Adams, T. Lian, R.B. Dyer, Balancing electron transfer rate and driving force for efficient photocatalytic hydrogen production in CdSe/CdS nanorod–[NiFe] hydrogenase assemblies, Energy Environ. Sci. 10 (2017) 2245–2255.
[9] Z. Li, Z. Sun, G. Zhang, Combining heterogeneous photocatalysis and enzymatic catalysis via membrane: conversion of biomass for H_2 production from water, Appl. Catal. B Environ. 338 (2023) 123069.
[10] J. Kim, Y.W. Lee, E.-G. Choi, P. Boonmongkolras, B.W. Jeon, H. Lee, S.T. Kim, S. K. Kuk, Y.H. Kim, B. Shin, Robust FeOOH/$BiVO_4$/Cu(In, Ga)Se_2 tandem structure

for solar-powered biocatalytic CO_2 reduction, J. Mater. Chem. A 8 (2020) 8496–8502.
[11] C. Feng, J. Rong, Y. Zhang, X. Zheng, X. Li, S. Xu, Z. Li, An S-scheme CeO_2/foveolate g-C_3N_4 composite with horseradish peroxidase activity for photo-enzyme synergistic catalytic degradation of phenanthrene, Appl. Catal. B Environ. 337 (2023) 123005.
[12] J. Wu, X. Ma, T. He, J. Han, Y. Zhu, C. Li, Y. Wang, A photo-enzyme coupling catalysis system with high enzyme loading for the efficient degradation of BPA in water, Sep. Purif. Technol. 313 (2023) 123392.
[13] G.A. Hutton, B.C. Martindale, E. Reisner, Carbon dots as photosensitisers for solar-driven catalysis, Chem. Soc. Rev. 46 (2017) 6111–6123.
[14] J. Shi, S. Fan, X. Li, P. Wang, Y. Mao, M. Wang, G. Chen, Artificial thylakoid membrane assisted $NiMn_2O_4$@PoPDA hierarchical hollow nanospheres for photo-enzyme integrated catalysis, Appl. Catal. B Environ. 342 (2024) 123434.
[15] J. Liu, X. Ren, C. Li, M. Wang, H. Li, Q. Yang, Assembly of COFs layer and electron mediator on silica for visible light driven photocatalytic NADH regeneration, Appl. Catal. B Environ. 310 (2022) 121314.
[16] H. He, X. Zhao, X. Jian, H. Zhang, T. Zeng, B. Feng, Y. Hu, Z. Yuan, X. Gao, F. Fu, Promoting photothermal catalytic CO_2 reduction of $Cd_2In_2S_5$/$Cd_{0.3}Zn_{0.7}S$ heterojunction with encapsulated hydrogen evolution active site by accelerating charge transfer kinetics, Chem. Eng. J. 476 (2023) 146442.
[17] H. He, X. Jian, T. Zen, B. Feng, Y. Hu, Z. Yuan, Z. Zhao, X. Gao, L. Lv, Z. Cao, Sulfur defect induced $Cd_{0.3}Zn_{0.7}S$ in-situ anchoring on metal organic framework for enhanced photothermal catalytic CO_2 reduction to prepare proportionally adjustable syngas, J. Colloid Interface Sci. 653 (2024) 687–696.
[18] R.K. Yadav, J.-O. Baeg, G.H. Oh, N.-J. Park, K.-j Kong, J. Kim, D.W. Hwang, S. K. Biswas, A photocatalyst–enzyme coupled artificial photosynthesis system for solar energy in production of formic acid from CO_2, J. Am. Chem. Soc. 134 (2012) 11455–11461.
[19] C.Y. Lee, H.S. Park, J.C. Fontecilla-Camps, E. Reisner, Photoelectrochemical H_2 evolution with a hydrogenase immobilized on a TiO_2-protected silicon electrode, Angew. Chem. Int. Ed. 55 (2016) 5971–5974.
[20] M.B. Wilker, J.K. Utterback, S. Greene, K.A. Brown, D.W. Mulder, P.W. King, G. Dukovic, Role of surface-capping ligands in photoexcited electron transfer between CdS nanorods and [FeFe] hydrogenase and the subsequent H_2 generation, J. Phys. Chem. C 122 (2018) 741–750.
[21] H. Jiang, X. Li, M. Li, P. Niu, T. Wang, D. Chen, P. Chen, J.-P. Zou, A new strategy for triggering photocatalytic activity of Cytrochrome P450 by coupling of semiconductors, Chem. Eng. J. 358 (2019) 58–66.
[22] S.S. Nadar, R.G. Pawar, V.K. Rathod, Recent advances in enzyme extraction strategies: a comprehensive review, Int. J. Biol. Macromol. 101 (2017) 931–957.
[23] S.P. France, L.J. Hepworth, N.J. Turner, S.L. Flitsch, Constructing biocatalytic cascades: in vitro and in vivo approaches to de novo multi-enzyme pathways, ACS Catal. 7 (2017) 710–724.
[24] Y.-Y. Yu, Y.-Z. Wang, Z. Fang, Y.-T. Shi, Q.-W. Cheng, Y.-X. Chen, W. Shi, Y.-C. Yong, Single cell electron collectors for highly efficient wiring-up electronic abiotic/biotic interfaces, Nat. Commun. 11 (2020) 4087.
[25] L.X. Xu, Y.Z. Wang, D. Zhou, M.Y. Chen, X.J. Yang, X.M. Ye, Y.C. Yong, Bio-metabolism-driven crystalline-engineering of CdS quantum dots for highly active photocatalytic H_2 evolution, ChemistrySelect 6 (2021) 3702–3706.
[26] R. Sanghi, P. Verma, A facile green extracellular biosynthesis of CdS nanoparticles by immobilized fungus, Chem. Eng. J. 155 (2009) 886–891.
[27] J.M. Jacob, S. Sharma, R.M. Balakrishnan, Exploring the fungal protein cadre in the biosynthesis of PbSe quantum dots, J. Hazard. Mater. 324 (2017) 54–61.
[28] K. Shivaji, S. Mani, P. Ponmurugan, C.S. De Castro, M. Lloyd Davies, M. G. Balasubramanian, S. Pitchaimuthu, Green-synthesis-derived CdS quantum dots using tea leaf extract: antimicrobial, bioimaging, and therapeutic applications in lung cancer cells, ACS Appl. Nano Mater. 1 (2018) 1683–1693.
[29] R. Lakshmipathy, N.C. Sarada, K. Chidambaram, S.K. Pasha, One-step, low-temperature fabrication of CdS quantum dots by watermelon rind: a green approach, Int. J. Nanomed. 10 (2015) 183–188.
[30] J. Sakizadeh, J.P. Cline, M.A. Snyder, C.J. Kiely, S. McIntosh, Biomineralization of nanocrystalline CdS/ZnS photocatalysts via controlled surface passivation for enhanced hydrogen evolution, ACS Appl. Nano Mater. 5 (2022) 2293–2304.
[31] T. Nonoyama, T. Kinoshita, M. Higuchi, K. Nagata, M. Tanaka, K. Sato, K. Kato, TiO_2 synthesis inspired by biomineralization: control of morphology, crystal phase, and light-use efficiency in a single process, J. Am. Chem. Soc. 134 (2012) 8841–8847.
[32] B. Wang, C. Zeng, K.H. Chu, D. Wu, H.Y. Yip, L. Ye, P.K. Wong, Enhanced biological hydrogen production from *Escherichia coli* with surface precipitated cadmium sulfide nanoparticles, Adv. Energy Mater. 7 (2017) 1700611.
[33] K.K. Sakimoto, A.B. Wong, P. Yang, Self-photosensitization of nonphotosynthetic bacteria for solar-to-chemical production, Science 351 (2016) 74–77.
[34] T.-X. Fan, S.-K. Chow, D. Zhang, Biomorphic mineralization: from biology to materials, Prog. Mater. Sci. 54 (2009) 542–659.
[35] Z. Nie, Y. Zhang, R. Tang, X. Wang, Biomimetic mineralization: an emerging organism engineering strategy for biomedical applications, J. Inorg. Biochem. 232 (2022) 111815.
[36] H. Shen, Y.-Z. Wang, G. Liu, L. Li, R. Xia, B. Luo, J. Wang, D. Suo, W. Shi, Y.-C. Yong, A whole-cell inorganic-biohybrid system integrated by reduced graphene oxide for boosting solar hydrogen production, ACS Catal. 10 (2020) 13290–13295.
[37] X. Xiao, X.-L. Ma, Z.-Y. Liu, W.-W. Li, H. Yuan, X.-B. Ma, L.-X. Li, H.-Q. Yu, Degradation of rhodamine B in a novel bio-photoelectric reductive system composed of *Shewanella oneidensis* MR-1 and Ag_3PO_4, Environ. Int. 126 (2019) 560–567.
[38] F. Mahmood, M. Shahid, S. Hussain, T. Shahzad, M. Tahir, M. Ijaz, A. Hussain, K. Mahmood, M. Imran, S.A.K. Babar, Potential plant growth-promoting strain *Bacillus sp.* SR-2-1/1 decolorized azo dyes through NADH-ubiquinone: oxidoreductase activity, Bioresour. Technol. 235 (2017) 176–184.
[39] Y. Li, X. Li, J. Li, J. Yin, Photocatalytic degradation of methyl orange by TiO_2-coated activated carbon and kinetic study, Water Res. 40 (2006) 1119–1126.
[40] F. Yang, Y. Jiang, M. Dai, X. Hou, C. Peng, Active biochar-supported iron oxides for Cr (VI) removal from groundwater: kinetics, stability and the key role of FeO in electron-transfer mechanism, J. Hazard. Mater. 424 (2022) 127542.
[41] S. Sharma, V. Dutta, P. Raizada, A. Hosseini-Bandegharaei, P. Singh, V.-H. Nguyen, Tailoring cadmium sulfide-based photocatalytic nanomaterials for water decontamination: a review, Environ. Chem. Lett. 19 (2021) 271–306.
[42] L. Cheng, Q. Xiang, Y. Liao, H. Zhang, CdS-based photocatalysts, Energy Environ. Sci. 11 (2018) 1362–1391.
[43] Y. Yin, C. Liu, G. Zhao, Y. Chen, Versatile mechanisms and enhanced strategies of pollutants removal mediated by *Shewanella oneidensis*: a review, J. Hazard. Mater. 440 (2022) 129703.
[44] W. Wang, Y. Tao, J. Fan, Z. Yan, H. Shang, D.L. Phillips, M. Chen, G. Li, Fullerene–graphene acceptor drives ultrafast carrier dynamics for sustainable CdS photocatalytic hydrogen evolution, Adv. Funct. Mater. 32 (2022) 2201357.
[45] X. Gao, H. He, W. Zhu, C. Yang, K. Xu, B. Feng, Y. Hu, F. Fu, Continuously flow photothermal catalysis efficiently CO_2 reduction over S-scheme 2D/0D Bi_5O_7I-OVs/$Cd_{0.5}Zn_{0.5}S$ heterojunction with strong interfacial electric field, Small 19 (2023) 2206225.
[46] Z. Yuan, H. He, X. Jian, H. Zhang, T. Zeng, R. Cao, Y. Hu, X. Gao, F. Fu, Synergistically enhanced photothermal catalytic CO_2 reduction by spatially separated oxygen and sulphur dual vacancy regulated redox half-reactions, J. Alloy. Compd. 968 (2023) 171959.
[47] G. Wang, K. Dou, H. Cao, R. Du, J. Liu, N. Tsidaeva, W. Wang, Designing Z-scheme CdS/WS_2 heterojunctions with enhanced photocatalytic degradation of organic dyes and photoreduction of Cr (VI): experiments, DFT calculations and mechanism, Sep. Purif. Technol. 291 (2022) 120976.
[48] X. Liu, J. Zhan, L. Liu, F. Gan, J. Ye, K.H. Nealson, C. Rensing, S. Zhou, In situ spectroelectrochemical characterization reveals cytochrome-mediated electric syntrophy in *Geobacter* coculture, Environ. Sci. Technol. 55 (2021) 10142–10151.
[49] L. Robuschi, J.P. Tomba, J.P. Busalmen, Proving *Geobacter* biofilm connectivity with confocal Raman microscopy, J. Electroanal. Chem. 793 (2017) 99–103.
[50] C.K. Ng, J. Xu, Z. Cai, L. Yang, I.P. Thompson, W.E. Huang, B. Cao, Elevated intracellular cyclic-di-GMP level in *Shewanella oneidensis* increases expression of c-type cytochromes, Microb. Biotechnol. 13 (2020) 1904–1916.
[51] M. Kataoka, A. Yamaoka, K. Kawasaki, Y. Shigeri, K. Watanabe, Extraordinary denaturant tolerance of keratinolytic protease complex assemblies produced by *Meiothermus ruber* H328, Appl. Microbiol. Biotechnol. 98 (2014) 2973–2980.
[52] C. Michaux, N.C. Pomroy, G.G. Privé, Refolding SDS-denatured proteins by the addition of amphipathic cosolvents, J. Mol. Biol. 375 (2008) 1477–1488.
[53] D.-M. Cao, X. Xiao, Y.-M. Wu, X.-B. Ma, M.-N. Wang, Y.-Y. Wu, D.-L. Du, Role of electricity production in the anaerobic decolorization of dye mixture by exoelectrogenic bacterium *Shewanella oneidensis* MR-1, Bioresour. Technol. 136 (2013) 176–181.
[54] Y. Honda, H. Hagiwara, S. Ida, T. Ishihara, Application to photocatalytic H_2 production of a whole-cell reaction by recombinant *Escherichia coli* cells expressing [FeFe]-hydrogenase and maturases genes, Angew. Chem. Int. Ed. 128 (2016) 8177–8180.
[55] B.S. Zuckerbraun, B.Y. Chin, M. Bilban, Jd.C. d'Avila, J. Rao, T.R. Billiar, L. E. Otterbein, Carbon monoxide signals via inhibition of cytochrome c oxidase and generation of mitochondrial reactive oxygen species, FASEB J. 21 (2007) 1099–1106.
[56] B. Kawahara, K.F. Faull, C. Janzen, P.K. Mascharak, Carbon monoxide inhibits cytochrome P450 enzymes CYP3A4/2C8 in human breast cancer cells, increasing sensitivity to paclitaxel, J. Med. Chem. 64 (2021) 8437–8446.